Biomaterials 54 (2015) 21–33

Contents lists available at ScienceDirect

Biomaterials

journal homepage: www.elsevier.com/locate/biomaterials

A transient cell-shielding method for viable MSC delivery within hydrophobic scaffolds polymerized *in situ*

Ruijing Guo [a, b], Catherine L. Ward [c], Jeffrey M. Davidson [d, e], Craig L. Duvall [f], Joseph C. Wenke [c], Scott A. Guelcher [a, b, f, *]

[a] Department of Chemical and Biomolecular Engineering, Vanderbilt University, Nashville, TN, USA
[b] Center for Bone Biology, Vanderbilt University Medical Center, Nashville, TN, USA
[c] US Army Institute of Surgical Research, Fort Sam Houston, TX, USA
[d] Department of Pathology, Microbiology and Immunology, Vanderbilt University, Nashville, TN, USA
[e] Research Service, VA Tennessee Valley Healthcare System, Nashville, TN, USA
[f] Department of Biomedical Engineering, Vanderbilt University, Nashville, TN, USA

ARTICLE INFO

Article history:
Received 8 September 2014
Received in revised form
26 February 2015
Accepted 4 March 2015
Available online 27 March 2015

Keywords:
Cell encapsulation
Polyurethane
Wound healing
Polymerisation
Mesenchymal stem cell
Polyorthoester

ABSTRACT

Cell-based therapies have emerged as promising approaches for regenerative medicine. Hydrophobic poly(ester urethane)s offer the advantages of robust mechanical properties, cell attachment without the use of peptides, and controlled degradation by oxidative and hydrolytic mechanisms. However, the application of injectable hydrophobic polymers to cell delivery is limited by the challenges of protecting cells from reaction products and creating a macroporous architecture post-cure. We designed injectable carriers for cell delivery derived from reactive, hydrophobic polyisocyanate and polyester triol precursors. To overcome cell death caused by reaction products from *in situ* polymerization, we encapsulated bone marrow-derived stem cells (BMSCs) in fastdegrading, oxidized alginate beads prior to mixing with the hydrophobic precursors. Cells survived the polymerization at >70% viability, and rapid dissolution of oxidized alginate beads after the scaffold cured created interconnected macropores that facilitated cellular adhesion to the scaffold *in vitro*. Applying this injectable system to deliver BMSCs to rat excisional skin wounds showed that the scaffolds supported survival of transplanted cells and infiltration of host cells, which improved new tissue formation compared to both implanted, pre-formed scaffolds seeded with cells and acellular controls. Our design is the first to enable injectable delivery of settable, hydrophobic scaffolds where cell encapsulation provides a mechanism for both temporary cytoprotection during polymerization and rapid formation of macropores post-polymerization. This simple approach provides potential advantages for cell delivery relative to hydrogel technologies, which have weaker mechanical properties and require incorporation of peptides to achieve cell adhesion and degradability.

1. Introduction

Autologous and allogeneic cell-based therapies have emerged as promising approaches for regenerative medicine [1]. While direct injection of cells has limited therapeutic efficacy due to poor cell survivability [2–4], delivery of cells within a 3D matrix can improve integration with host tissue and promote healing [5]. Injectable and settable cell carriers could be advantageous as a minimally invasive surgical approach to rapid filling of complex defects followed by *in situ* curing to form a porous scaffold with suitable mechanical properties [6].

Lysine-derived poly(ester urethane)s (PURs) offer potential advantages as injectable carriers for local cell delivery, such as curing using non-cytotoxic catalysts [7] without the need for UV radiation [8], support of cell attachment without cell adhesion peptides [9,10], tunable hydrolytic and oxidative degradation to non-cytotoxic breakdown products [11,12], and adjustable mechanical properties ranging from those of soft tissue [13] to bone [9,14]. Furthermore, macropores can be generated within PUR scaffolds by CO_2 gas foaming via the reaction of isocyanate groups with water [15]. When using these materials as acellular scaffolds, the CO_2 and

* Corresponding author. Department of Chemical and Biomolecular Engineering, Vanderbilt University, Nashville, TN, USA.
E-mail address: scott.guelcher@vanderbilt.edu (S.A. Guelcher).

http://dx.doi.org/10.1016/j.biomaterials.2015.03.010
0142-9612/

Report Documentation Page

Form Approved
OMB No. 0704-0188

1. REPORT DATE	2. REPORT TYPE	3. DATES COVERED
01 JUN 2015	**N/A**	**-**

4. TITLE AND SUBTITLE	5a. CONTRACT NUMBER
A transient cell-shielding method for viable MSC delivery within hydrophobic scaffolds polymerized in situ	5b. GRANT NUMBER
	5c. PROGRAM ELEMENT NUMBER
6. AUTHOR(S)	5d. PROJECT NUMBER
Guo, Ruijing; Ward, Catherine L.; Davidson, Jeffrey M.; Duvall, Craig L.; Wenke, Joseph C.; Guelcher, Scott A.;	5e. TASK NUMBER
	5f. WORK UNIT NUMBER
7. PERFORMING ORGANIZATION NAME(S) AND ADDRESS(ES)	8. PERFORMING ORGANIZATION REPORT NUMBER
United States Army Institute of Surgical Research, JBSA Fort Sam Houston, Tx 78234	
9. SPONSORING/MONITORING AGENCY NAME(S) AND ADDRESS(ES)	10. SPONSOR/MONITOR'S ACRONYM(S)
	11. SPONSOR/MONITOR'S REPORT NUMBER(S)

12. DISTRIBUTION/AVAILABILITY STATEMENT
Approved for public release, distribution unlimited

13. SUPPLEMENTARY NOTES

14. ABSTRACT

15. SUBJECT TERMS

16. SECURITY CLASSIFICATION OF:			17. LIMITATION OF ABSTRACT	18. NUMBER OF PAGES	19a. NAME OF RESPONSIBLE PERSON
a. REPORT	b. ABSTRACT	c. THIS PAGE			
unclassified	**unclassified**	**unclassified**	**SAR**	**13**	

heat generated by the *in situ* reaction is well tolerated at the biomaterial–tissue interface [7,16] due to the relatively long length scales (>1 mm) between the material and surrounding cells (Fig. 1A). However, cells encapsulated within the reactive hydrophobic polymer experience steeper CO_2 and temperature gradients due to transport of reaction products over much smaller length scales (<100 μm, Fig. 1A). Furthermore, after the reaction is complete, hydrophobic polymers absorb negligible amounts of water and allow less diffusion of vital cell nutrients and wastes than swollen hydrogels. While hydrophobic biomaterials such as PUR provide a generalizable, biodegradable platform for tissue scaffolding, their use as an injectable carrier for cell delivery has not been achieved due to two primary challenges: (1) maintenance of cell viability during *in situ* polymerization, and (2) provision of an interconnected, macroporous structure to allow effective nutrient and waste exchange post-cure. Overcoming these key barriers was the goal of the current work in order to enable the use of injectable, settable, mechanically robust, and cell-adhesive PUR networks to fill tissue defects and to locally deliver and retain viable cells *in vivo*.

Achieving these goals will provide a new alternative to photopolymerizable systems that utilize cytocompatible initiators [17,18] and water-soluble macromers [19–21] to encapsulate cells in injectable hydrogels [8]. Polyethylene glycol (PEG)-based hydrogels have generated considerable interest for localized cell delivery since they can be administered by minimally-invasive injections, set within clinically relevant working times, exhibit tissue-like structure, and induce a minimal inflammatory response [1,22–24]. However, PEG hydrogels must be functionalized with an optimal combination of peptides that serve as integrin-binding sites for cell adhesion and peptide crosslinkers that are matrix metalloproteinase (MMP) substrates to enable cellular infiltration and cell-mediated hydrogel degradation [5,25].

Alternative settable carriers must protect cells from reaction products prior to cure and then set *in situ* to form an interconnected, macroporous scaffold that supports cell adhesion and growth. In this study, we designed injectable PUR scaffolds for concurrent incorporation of macropores and cells within PUR scaffolds (Fig. 1B). Through encapsulation within partially oxidized sodium alginate (o-Alg) beads, cells were protected from the PUR reaction prior to gelation. Hydrolytic degradation of the o-Alg beads within the first 1–2 days after gelation was anticipated to result in cell release and attachment to the scaffold. Thus, in contrast to the porogen co-encapsulation approach [26,27], the o-Alg beads functioned both as a temporary barrier to transport of reaction products as well as a porogen. We varied bead size, timing of bead addition, and bead loading within PUR scaffolds to investigate the effects of heat and CO_2 generation on cell survivability both prior to and after gelation *in vitro*. In a proof-of-concept experiment, the lead-candidate formulation that produced maximal cell survivability *in vitro* was injected into full-thickness excisional skin wounds in Sprague–Dawley rats to evaluate the potential of the injectable PUR cell carrier for wound repair and restoration.

2. Materials and methods

2.1. Materials

The sodium salt of alginic acid (Alg, viscosity = 20–40 cPs) was supplied by Sigma Aldrich (St. Louis, MO). Acros Organics supplied calcium chloride and glycerol. αMEM and DMEM were supplied by GIBCO. Fetal bovine serum (FBS) was purchased from Thermo Scientific. Penicillin/streptomycin (P/S), trypsin EDTA and Amphotericin B were obtained from Corning Cellgro. Live/Dead kits for mammalian cells were supplied by Life Technologies. Glycolide and D,L-lactide were purchased from Polysciences (Warrington, PA). Lysine triisocyanate-poly(ethylene glycol) (LTI-PEG) prepolymer was supplied by Medtronic, Inc, and hexamethylene diisocyanate trimer (HDIt) was supplied by Bayer Material Science. Iron acetylacetonate (FeAA) was supplied by Sigma–Aldrich. ε-caprolactone was dried over anhydrous $MgSO_4$, and all other materials were used as received.

2.2. Cell culture

MC3T3 cells (ATCC) were cultured in a complete medium of αMEM with 10% FBS and 1% P/S. Primary rat bone marrow mesenchymal stem cells (BMSCs) were maintained in DMEM with 10% FBS, 1% P/S, and 0.1% Amphotericin B (Sigma). BMSCs were generated from pooled bone marrow from 4 male Sprague–Dawley rats. Rat femora and tibiae were removed after sacrificing and bone marrow flushed with BMSC culture medium. After centrifuging, cell pellets were suspended in BMSC medium and plated in T75 tissue culture flasks. Three days after seeding, floating

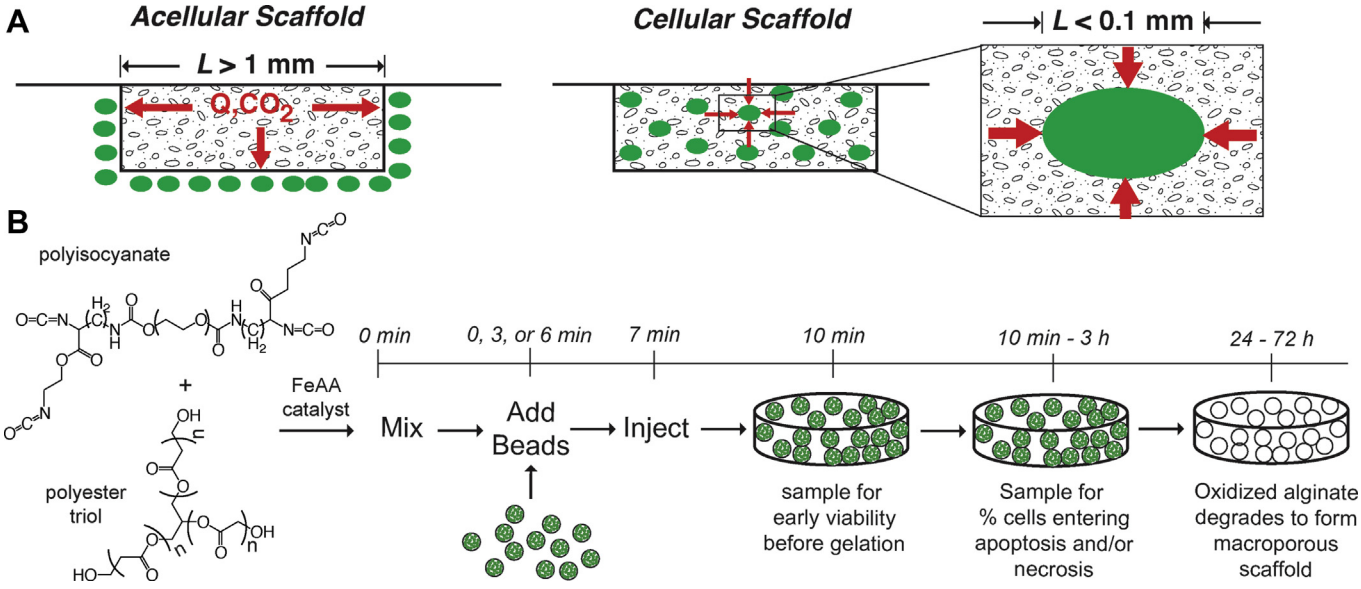

Fig. 1. Design of injectable, settable carriers for cell delivery. (A) For an acellular scaffold, the length scale of diffusion of reaction products is comparable to the size of the tissue defect. However, in a cellular scaffold, reaction products diffuse radially toward the encapsulated cell over a much shorter length scale (comparable to the size of the cell). (B) Schematic illustrating the design concept in which an NCO-functional prepolymer reacts with a polyester polyol in the presence of an iron acetylacetonoate (FeAA) catalyst to form a polyurethane network. Encapsulation of cells in oxidized alginate beads (green) provides temporary protection from the chemical reaction and is followed by hydrolytic degradation of the oxidized alginate to form interconnected macropores that are enhanced by the NCO-water reaction. (For interpretation of the references to color in this figure legend, the reader is referred to the web version of this article.)

cells were removed and culture medium refreshed every other day. BMSCs were differentiated to osteoblasts and adipocytes (Fig. S1) to confirm their pluripotency.

2.3. Preparation of partially oxidized alginate

Partially oxidized sodium alginate (o-Alg) degrades significantly faster than untreated Alg [28]. Furthermore, o-Alg has been reported to induce negligible inflammation and oxidative stress responses in cells [29], and it does not react with PUR to generate radicals (Fig. S2). These properties underscore its potential utility as a temporary barrier to shield cells from harmful reaction products. An aqueous solution of sodium periodate (2.0 mM) was mixed with 1 w/v% solution of sodium alginate (Alg) and reacted in the dark for 24 h at ambient temperature. Two drops of ethylene glycol were added to stop oxidation. The resultant solution was precipitated in ethanol (2:1 v/v ethanol/water) and sodium chloride (6.25 g/L). Precipitates were dissolved in distilled water to the original volume, precipitated in ethanol solution, and dried under vacuum at room temperature. After drying, partially oxidized sodium alginate (o-Alg) was dissolved in distilled water, filtered, and lyophilized [28]. A concentration of 4 w/v% of o-Alg was utilized to generate hydrogel beads.

2.4. Encapsulation of cells in alginate beads

Cells (10^5 cells/mL) were encapsulated in calcium alginate hydrogel by pumping the sodium alginate solution (1 w/v% for Alg and 4 w/v% for o-Alg) through a nozzle (0.35 μm diameter) into a 100 mM calcium chloride crosslinking solution. An electronic bead maker (Nisco, VAR V1) was used to control bead size over the range 300–2000 μm by adjusting the potential difference between the nozzle and gelling agent solution [30]. Alginate bead size was measured by light microscopy.

2.5. Synthesis and characterization of polyurethane scaffolds

A polyester triol (900 g/mol) was synthesized from a glycerol starter and a backbone comprising 70 wt% ε-caprolactone, 20 wt% glycolide, and 10 wt% D,L-lactide as described previously [31]. An isocyanate (NCO)-terminated prepolymer (21,000 cP, NCO:OH equivalent ratio = 3.0:1.0, 21% NCO [32]) was synthesized by adding polyethylene glycol (PEG, 200 g/mol) drop-wise to lysine triisocyanate (LTI). Polyurethane (PUR) scaffolds were synthesized by reactive liquid molding of the prepolymer with a hardener component comprising the polyester triol, iron catalyst (5% iron acetylacetonate (FeAA) in dipropylene glycol), and alginate beads. The reactivity of the LTI-PEG prepolymer was measured by using ATR-FTIR (Bruker, Billerica, MA) to quantify the disappearance of the NCO peak [7]. Rheological properties of the scaffolds during curing process were measured with a parallel plate AR 2000ex rheometer in dynamic mode (New Castle, DE) to determine the working time (crossover point of storage moduli (G′) and loss moduli (G″)).

For porosity, permeability, and mechanical measurements, scaffolds were prepared using o-Alg beads followed by 48 h incubation in PBS to dissolve the o-Alg and vacuum drying. Pore morphology and size distribution were determined by SEM (Hitachi, Finchampstead, UK). Porosity was calculated from mass and volume measurements of cylindrical scaffold cores (ρ_{PUR} = 1.27 g cm^{-3}) [15]. Young's modulus was determined from the slope of the stress–strain curve from compression tests performed using a TA Instruments Dynamic Mechanical Analyzer Q1000 (New Castle, DE). The flow rate of air through the scaffold was measured using a flowmeter and the permeability calculated as:

$$k = Q\frac{L}{A}\left(\frac{\mu}{\Delta P}\right) \quad (1)$$

where Q = volumetric air flow rate, L and A are the scaffold thickness and cross-sectional area, μ is the viscosity of air, and ΔP is the pressure drop across the scaffold [33].

2.6. Effects of bead size on survival of encapsulated cells during polymerization

The ability of cells to survive the polymerization was evaluated at 30 min after mixing of the polyisocyanate and polyester triol components. At this early time point, conduction of heat and diffusion of CO_2 into the beads, which occur on the time scale of minutes, were anticipated to be the primary regulators of cell survival. Alg beads (500–2000 μm) containing cells were added to the LTI-PEG prepolymer, polyester triol, and catalyst (0.26 wt% FeAA) at a loading of 50%. Beads were removed from the scaffolds at 30 min post-mixing using forceps, washed with Dulbecco's Phosphate Buffered Saline (DPBS, Corning, Corning, NY), and stained with the Cytotoxicity Kit (Live/Dead® Viability/Cytotoxicity Kit for mammalian cells, Invitrogen). An inverted confocal microscope (Zeiss LSM 510) was used to capture a series of Z-stack images of the 3D beads. The number of live ($N_{live,}$ green) and the total number of cells (N_{total}, the number of all stained cells, including both live and also yellow, orange, and red dead or damaged cells) in each image were counted. Cell viability was calculated as [34]:

$$\%\text{Viability} = \frac{N_{live}}{N_{total}} \times 100\% \quad (2)$$

2.7. Survival of encapsulated cells at early time points prior to gelation

Preliminary experiments revealed evidence of acute cell death when cells were encapsulated in 500 μm beads, presumably due to transport of PUR reaction products into the beads. Therefore, the polyisocyanate composition (LTI-PEG or HDIt), timing of 500 μm bead addition (0, 3, or 6 min delay), and catalyst concentration (0, 0.26, or 0.52 wt% FeAA) were varied to control the amount of cell exposure to heat and CO_2. The study design is summarized in Table 1. The viability of cells embedded in non-reactive controls with no catalyst (L-0C-0) was also measured to decouple any effects of chemical toxicity from loss of cell viability due to reaction-generated heat and CO_2. Beads containing cells were removed from the cured scaffolds at 10 min using forceps and analyzed for cell viability (V_{10}) as described above.

2.8. Survival of encapsulated cells at later time points after gelation

At later time points after gelation, both exposure to reaction products as well as the permeability of the scaffold, which controls transport of nutrients and wastes into the scaffold, could limit cell survivability. Therefore, cell survivability was investigated as a function of bead loading (50 or 70% 500 μm Alg beads) and timing of bead addition (0 or 3 min delay) at 10 min (prior to gelation), 30 min (at gelation), and 3 h (after gelation) post-mixing. At each time point, Alg beads containing cells were removed from the cured scaffolds and stained with an Apoptotic & Necrotic Cell Differentiation kit (PromoCell GmbH). Apoptotic cells were identified with fluorescein- (FITC, green) labeled Annexin V, necrotic cells were identified with a positively charged nucleic acid probe Ethidium homodimer III (EthD-III, red), and Hoechst 33342 (blue) was used to identify the total number of cells. An inverted fluorescence microscope (Olympus CKX41) was used to identify healthy cells (blue) as well as cells entering apoptosis (blue and green) or necrosis (blue, green, and red). The percentage of cells entering necrosis or apoptosis was calculated using Eq. (2). In another test group, the porosity and permeability of the scaffolds were measured (except for the 70% immediate addition group, which were too friable to be tested).

2.9. Culture of cellularized PUR scaffolds

Rat BMSCs were stained with a cytoplasmic dye (VyBrant® CFDA SE Cell Tracer Kit, Life Technologies, per the manufacturer's guidelines), encapsulated in Alg or o-Alg beads, embedded in PUR scaffolds, and cultured in 48-well tissue culture plates for 1, 4, and 7 days. Scaffolds were rinsed with DPBS and fixed with 5% glutaraldehyde or 2% OsO_4 solution before vacuum drying for SEM imaging. A subset of scaffolds was also sectioned (30 μm) for microscopic imaging to observe cell viability and attachment to the scaffolds, which were cut open to expose the interior.

Table 1
Experimental conditions for measurement of early-stage (10 min) cell survivability. Values of $n_{CO2,10}$ (CO_2 generated by the reaction at 10 min) and Q_{10} (heat generated by the reaction at 10 min) were calculated from the PUR reaction kinetics model. Alginate beads were removed from the scaffolds 10 min after the start of mixing and cell viability measured (V_{10}).

Treatment group	Isocyanate	FeAA catalyst wt%	Delay min	$n_{CO2,10}$ mmol cm^{-2}	Q_{10} J cm^{-2}	Rate const. g eq^{-1} min^{-1}	k_G/k_W
L-0C-0	LTI-PEG	0%	0	0	0	N/A	N/A
L-5C-0	LTI-PEG	0.26%	0	0.107	0.392	k_G = 12.1	6.4
L-5C-3	LTI-PEG	0.26%	3	0.085	0.380	k_B = 1.9	
L-5C-6	LTI-PEG	0.26%	6	0.063	0.367		
H–5C-0	HDIt	0.26%	0	0.044	0.317	k_G = 8.2 k_B = 0.61	13.4
H–10C-0	HDIt	0.52%	0	0.036	0.655	k_G = 31.4 k_B = 0.68	46.2

Scaffolds were fixed in 10% formalin for 15 min, washed in PBS, and dehydrated through increasing alcohol concentrations (50–100%). Materials were air-dried and mounted to a specimen stub using carbon tape. Samples were sputter-coated with gold (108 Auto Sputter Coater; TedPella, Redding CA) and viewed via SEM (Carl Zeiss VP-40; Oberkochen, Germany). The ability of the MSCs to retain pluripotency after embedding in the scaffolds was determined by measuring adipogenic and osteogenic differentiation. Scaffolds were maintained in growth, adipogenic, or osteogenic media for up to 21 days and stained with Oil Red O or Alizarin Red S. After staining, dyes were dissolved in appropriate solvents (100% isopropanol for Oil Red O and 5% SDS for Alizarin Red S) and absorbances of the solutions were read on a plate reader (OD 490 nm for Oil Red O and OD 570 nm for Alizarin Red S). Absorbances were compared to stained scaffolds cultured in growth media.

2.10. In vivo cutaneous repair in rats

All surgical and care procedures were carried out under aseptic conditions per an approved Institutional Animal Care and Use Committee (IACUC) protocol. Scaffolds ($n = 4$) that contained encapsulated male rat BMSCs were injected into 10 mm full-thickness excisional wounds in the dorsal skin of adult female Sprague–Dawley rats and allowed to cure for 15 min [16]. BMSCs encapsulated in Alg beads and embedded in PUR scaffolds did not integrate with host tissue and were consequently ejected from the wound bed. Therefore, only scaffolds containing o-Alg beads were evaluated. Injectable scaffolds containing no cells (Inj group) and implanted, preformed scaffolds seeded with cells (Impl + BMSC group) were both evaluated as controls compared to injectable scaffolds with cells (Inj + BMSC). Rats were euthanized 4d and 7d after surgery and the wounds harvested for histology and qRT-PCR. RNA from each sample was isolated and purified by RNeasy Mini Kit (Qiagen). cDNA synthesis was carried out from purified total RNA using iScript™ Reverse Transcription Supermix (Biorad). RT-PCR amplified for rat SRY gene (5′-CATCGAAGGGTTAAAGTGCCA-3′, 5′ – ATAGTGTGTAGGTTGTTGTCC-3′) was measured to track the fate of delivered cells. Gomori's trichrome staining and Ki67 and collagen IV immunostaining were performed on tissue sections for tissue infiltration, cell proliferation and angiogenesis analysis, respectively. The ROI (region of interest) for quantitative analysis of tissue infiltration comprised a rectangle centered between the midpoint and the edge of the excisional wound. The reactivity was expressed as the percentage of area occupied by immunoreactive cells.

2.11. Statistical analysis

The statistical significance between experimental groups was determined by a two-factor ANOVA. Graphs show mean ± standard deviation. $p \leq 0.05$ was considered statistically significant.

3. Results

3.1. Reactivity and settability

Injectable reactive liquid precursors that cure *in situ* to form a solid scaffold should ideally be amenable to flow through a small-bore needle and set within clinically relevant gelation times to form a polymer network with suitable mechanical properties [35–37]. The gel point approximates the working time available for injection, since beyond the gel point the mixture is no longer flowable. For a prepolymer with functionality of 4 and a polyol with functionality of 3, the gel point occurs at $\xi_{GP} = 38\%$ conversion of the reactive NCO groups [38], which was achieved at 25.5 min when cell-containing beads were immediately added to the reactive PUR mixture (Fig. 2A). Since CO_2 generated during the polymerization might harm the cell-loaded beads added to the reactive mixture, the effects of delaying the addition of the beads were also investigated. When addition of beads to the reactive PUR was delayed for 3 min, the gel point decreased to 19.5 min (Fig. 2A). The working time can also be determined by the G′-G″ crossover point (Fig. 2B, C), at which point the storage modulus (G′) equals the loss modulus (G″). For delayed addition, the crossover point occurred at 22 min, which is comparable to that determined from chemical reaction kinetics (Fig. 2A). In contrast, for immediate addition, the crossover point occurred at 33 min (both G′ and G″ decreased with time at early time points due to significant volumetric expansion of the scaffold as a result of CO_2 generation (Fig. 2C).

3.2. Effects of bead size on cell survival at gelation

MC3T3 cells were encapsulated in Alg beads that were immediately mixed (0 min delay, 50% loading) with the reactive PUR. Beads were harvested from the scaffolds after 30 min and stained for live and dead cells. For 500–2000-μm diameter beads not embedded in PUR, the viability of encapsulated MC3T3 cells exceeded 95% and was independent of bead size (Fig. 3A, C). However, when embedded in the reactive PUR (Fig. 4B), cell viability decreased with decreasing bead size (Fig. 3C). These observations suggest that transport of heat and/or CO_2 generated by the PUR reaction reduced cell survival prior to gelation.

3.3. Effects of delayed addition of MSCs on acute cell survivability at early time points

As shown in Fig. 3, survival of MC3T3 cells encapsulated in 500 μm Alg beads was only 30%, presumably due to exposure of cells to PUR reaction products. The timing of bead addition (0, 3, or 6 min delay), the isocyanate composition (LTI-PEG or HDIt), and the catalyst concentration (0, 0.26, or 0.52 wt% FeAA) were varied to control the amount of heat (Fig. 4A) and CO_2 (Fig. 4B) generated by the PUR gelling (k_G) and blowing (k_B) reactions. The NCO groups in the polyisocyanate (R_1-NCO) react with hydroxyl groups (OH) in the polyester triol (R_2-OH) by the gelling reaction or in water (W) by the blowing reaction:

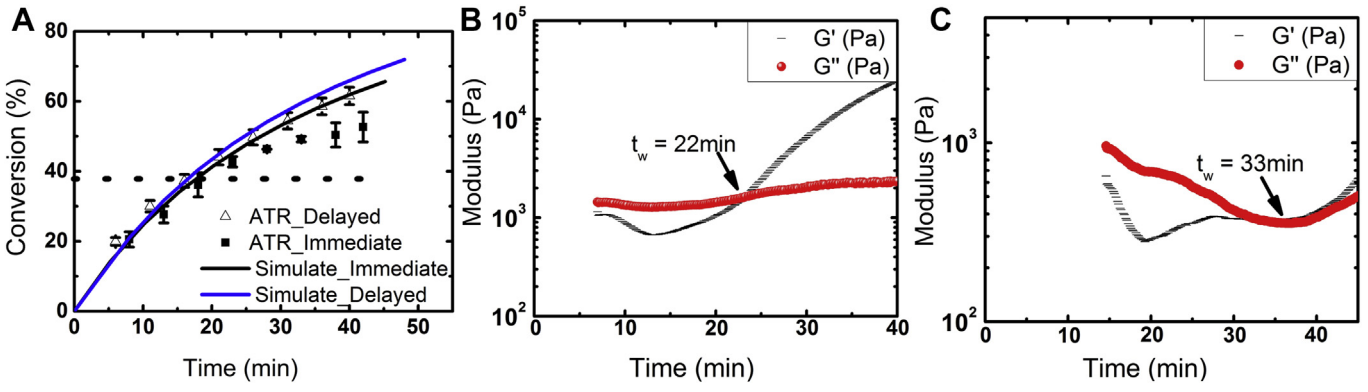

Fig. 2. Handling properties of injectable and settable PUR scaffolds. (A) Overall NCO conversion for immediate and delayed (3 min) addition of alginate beads. The gel point (working time t_w) occurred at 38% NCO conversion (dashed line), which corresponded to 19.5 min for delayed addition and 25.5 min for immediate addition. (B–C) Storage (G′) and loss (G″) moduli versus time for delayed (3 min, B) and immediate (0 min, C) addition of alginate beads. The value of t_w is defined as the G′–G″ crossover point (22 min for delayed addition).

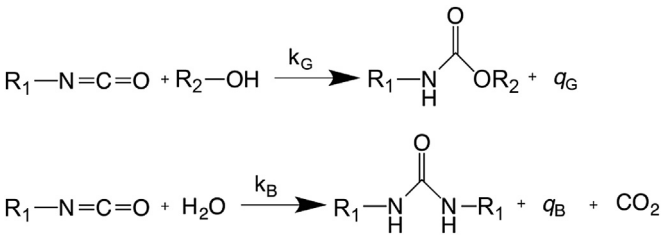

(3)

The amounts of heat (q_G or q_B) and CO_2 generated by Reaction (3) at 10 min were calculated from a PUR reaction kinetics model [7] (Q_{10} and $n_{CO2,10}$ listed in Table 1). Cell viability was measured at 10 min (V_{10}) to test the hypothesis that transport of heat and/or CO_2 is the primary cause of acute cell death prior to gelation. The rates of the second-order gelling (r_G) and blowing (r_B) reactions are given by:

$$r_G = k_G C_{NCO} C_{OH,P}$$
$$r_B = k_B C_{NCO} C_{OH,W} \quad (4)$$

where C_{NCO} is the concentration of NCO groups in the prepolymer (eq g^{-1}) and C_{OH} is the concentration of OH groups (eq g^{-1}) in the polyester triol (P) or water (W). The specific reaction rates k_G and k_B (Table 1) were calculated from kinetic experiments in which the polyisocyanate was reacted with either the polyester triol (k_G) or water (k_B) and the disappearance of the NCO peak monitored by ATR-FTIR over time [7,39].

The concentration profiles of each component were calculated as a function of time by modeling the system as a constant-volume isothermal batch reactor, since the increase in temperature in the bulk scaffold was <15°C [15]. The equivalent balance equations for polyester triol and water were solved $C_{OH,P}$ and $C_{OH,W}$ using the ode45 function in MATLAB:

$$\frac{dC_{OH,P}}{dt} = -r_G M_{PUR}, \quad t = 0,\ C_{OH,P} = C_{OH,P0}$$
$$\frac{dC_{OH,W}}{dt} = -r_B M_{PUR}, \quad t = 0,\ C_{OH,W} = C_{OH,W0} \quad (5)$$

where M_{PUR} is the mass of the PUR component (polyisocyanate and polyester triol) and $C_{OH,P0}$ and $C_{OH,W0}$ denote the initial concentrations (eq g^{-1}) of polyester triol and water, respectively (details of how these parameters were determined are described in the Supplemental Information).

The heat generated by the gelling and blowing reactions as a function of time was normalized by the total alginate (A) bead area (Q, J cm^{-2}). The CO_2 generated by the blowing reaction was also normalized by the alginate bead area (mmol CO_2 cm^{-2}):

$$Q = \frac{\Delta H_{Rx} a_A \rho_A (1 - x_A)}{3 x_A} \left(\frac{C_{OH,P0} - C_{OH,P}}{f_P} - \frac{C_{OH,W0} - C_{OH,W}}{f_W} \right)$$
$$n_{CO_2} = \frac{a_A \rho_A (1 - x_A)}{3 x_A} \left(\frac{C_{OH,W0} - C_{OH,W}}{f_W} \right) \quad (6)$$

where f is the functionality (eq mol^{-1}), ΔH_{Rx} = 80 kJ mol^{-1} is the heat of reaction [40], a_A is the radius of the alginate beads, ρ_A = 1.601 g cm^{-3} is the density of alginate, and x_A is the weight fraction of alginate beads in the scaffold. The values of Q and n_{CO2} are plotted versus time in Fig. 4A–B. The amounts of heat (Q_{10}) and CO_2 ($n_{CO2,10}$) generated at 10 min are listed in Table 1. The effects of Q_{10} and $n_{CO2,10}$ on cell viability (V_{10}) are shown in the contour plot in Fig. 4C. The values of V_{10} were fit to the following equation to generate the contour plot:

$$V_{10} = 87.7 - 0.0883 \exp(56.35 n_{CO_2,10}) - 1.34 \exp(3.76 Q_{10}) \quad (7)$$

Mixing the beads with a non-reactive PUR mixture (LTI-PEG or HDIt) reduced the viability to 88%, which is about 10% less than that measured for the beads alone. Thus, for the region bounded by Q_{10} < 0.4 J cm^{-2} and $n_{CO2,10}$ < 0.08 mmo cm^{-2}, the effects of the chemical reaction on cell viability were negligible. However, outside this range, V_{10} decreased exponentially with Q^*_{10} and

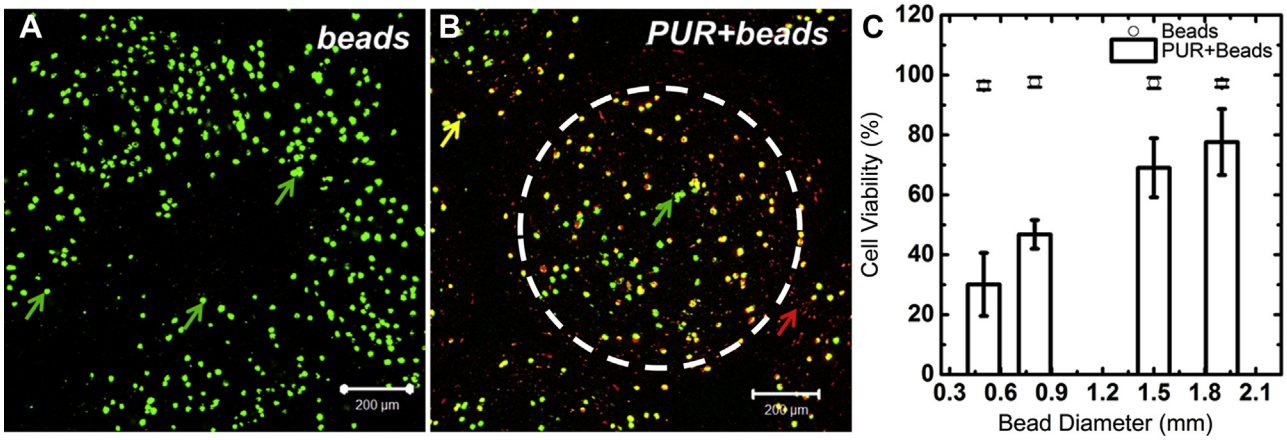

Fig. 3. Effects of bead size on survival of MC3T3 cells encapsulated in Alg beads and embedded in injectable PUR scaffolds at early time points (10 min post-mixing). (A) Confocal images show viable (green) cells in 500 μm beads. (B) Viability decreases when viable (green) MC3T3 cells encapsulated in Alg are immediately embedded in PUR scaffolds prepared from LTI-PEG (L-5C-0 group, Table 1). Immediate embedding of Alg beads in PUR scaffolds resulted in significant cell death (yellow, orange, and red cells) near the surface of the beads. (C) The viability of encapsulated cells immediately embedded in PUR scaffolds correlated with bead size, suggesting that transport of reaction products into the beads was responsible for the observed cytoxicity. (For interpretation of the references to color in this figure legend, the reader is referred to the web version of this article.)

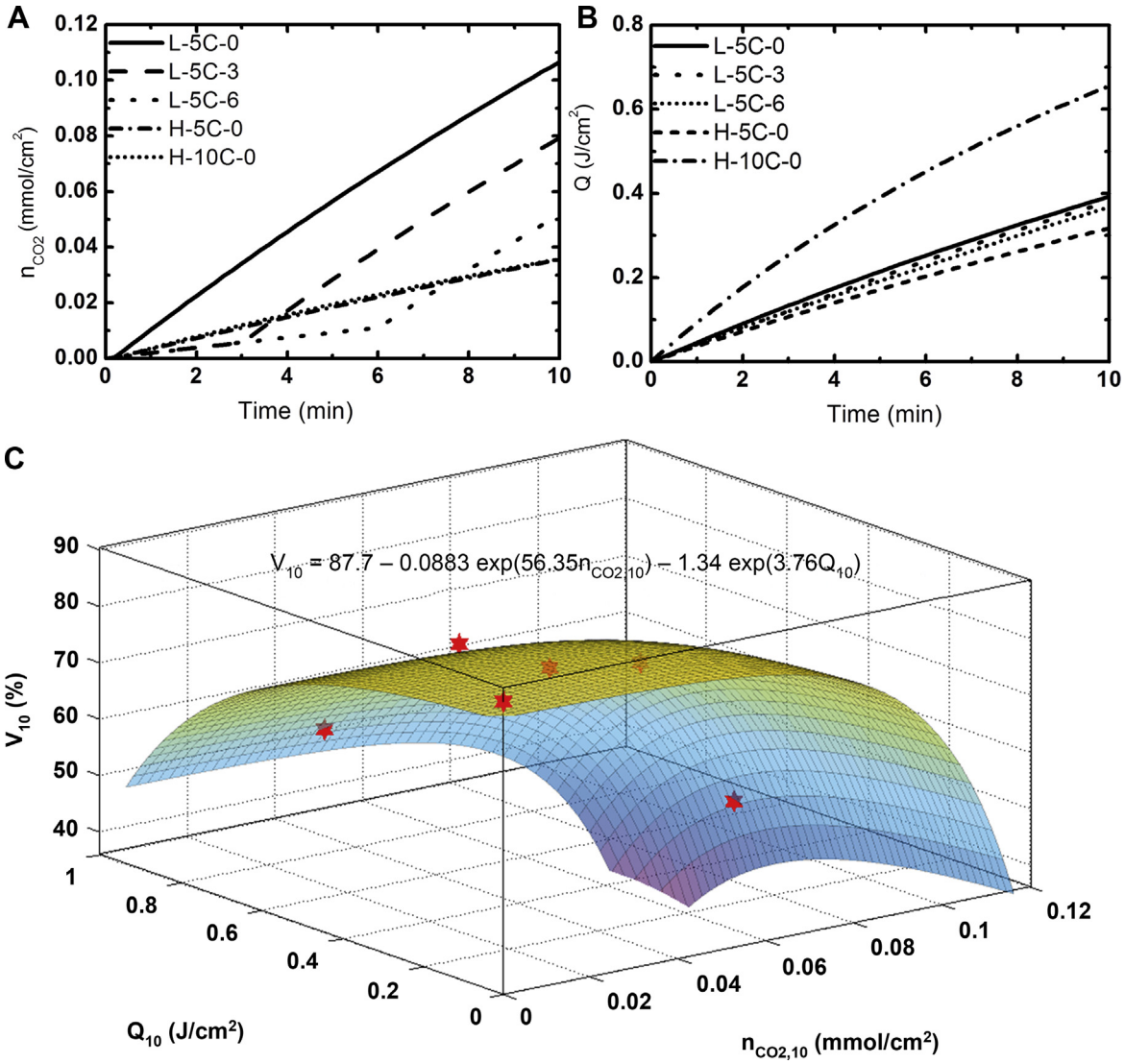

Fig. 4. Effects of heat and CO_2 released by the PUR reaction on viability of MSCs encapsulated in Alg beads and embedded in a reactive hydrophobic polymer at early time points. (A) Plot of the moles CO_2 generated by the PUR reaction (n_{CO2}, calculated from the reaction kinetics model) as a function of time for up to 10 min. (B) Plot of the heat generated (Q, calculated from the reaction kinetics model) as a function of time for up to 10 min. (C) Contour plot showing V_{10} as a function of CO_2 ($n_{CO2,10}$) and heat (Q_{10}) generated at 10 min. Red stars represent the data points and the surface was plotted from the fit to the experimental data shown on the plot. (For interpretation of the references to color in this figure legend, the reader is referred to the web version of this article.)

$n^*_{CO2,10}$. Taken together, these data indicate that CO_2 diffusion and heat conduction into the beads contributed to acute cell death prior to gelation.

3.4. Effects of permeability on cell survival at later time points after gelation

After gelation (20–30 min, Fig. 1), the reactive PUR cures to form an elastomeric scaffold. Permeability (Eq. (1)) and porosity are key parameters controlling the rate of transport of nutrients into the scaffold. Thus, the effects of bead loading and the timing of bead addition on the porosity, permeability, and mechanical properties of the PUR scaffolds were investigated. SEM images comparing scaffolds prepared by 3 min delayed addition of o-Alg beads at 50 wt versus 70 wt% (Fig. 5A–B) supported this hypothesis and showed that pore connectivity increased with bead loading. As bead loading increased from 50 to 70 wt% (3 min delay), the increase in porosity was not significant (78–82%), but the air permeability increased five-fold ($p < 0.05$, Fig. 5C) to values comparable to those reported for open-pore PUR foams with similar densities [33]. In contrast, when the beads were added immediately (0 min delay), neither permeability nor porosity increased with bead loading (Fig. 5D). This observation suggests that CO_2 gas foaming controlled porosity and permeability when the beads were immediately added to the PUR. The elastic modulus (E^*) of scaffolds prepared by immediate or delayed addition of beads followed the predicted scaling with porosity ε (Fig. 5E) [41]:

$$E^* = E_s\left(\frac{1-\rho_s\varepsilon}{\rho_s}\right)^2 \tag{8}$$

where the density of the bulk polymer $\rho_s = 1.27$ g cm^{-3} and the modulus of the bulk polymer $E_s = 2.5$ MPa.

The data in Fig. 2–4 point to transport of heat or CO_2 into the Alg beads as a key factor contributing to acute cell death prior to gelation. After gelation, cells may undergo apoptosis or necrosis due to the continuing effects of the chemical reaction and/or hindered transport into the interior of the scaffold. To investigate the

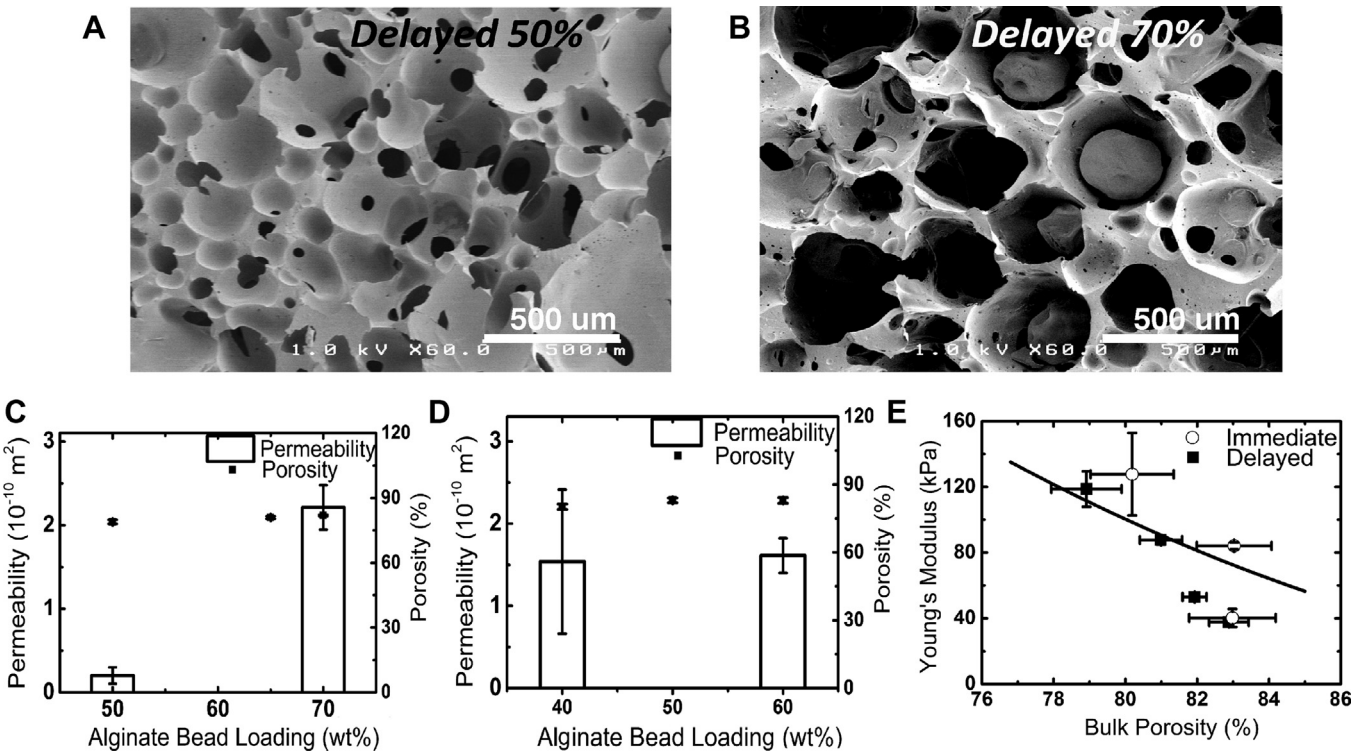

Fig. 5. Effects of bead loading and timing of bead addition on PUR scaffold properties. (A–B) Representative SEM images of scaffolds fabricated with (A) 50 wt% o-Alg beads and (B) 70 wt% o-Alg beads. (C, D) Porosity and permeability of PUR scaffolds as a function of o-Alg bead loading for (C) delayed (3 min) and (D) immediate addition. (E) The elastic modulus of the scaffolds prepared by delayed and intermediate addition of beads decreased with bulk porosity.

relative contributions of the chemical reaction and scaffold permeability to cell survivability, Alg beads were removed from the cured scaffolds at 10 min (prior to the gel point), 30 min (at the gel point), and 3 h (after the gel point) using forceps and stained to identify apoptosis and necrosis. Plots of the percentage of cells undergoing apoptosis (Fig. 6A) or necrosis (Fig. 6B) versus time reveal that the number of cells entering apoptosis or necrosis did not change substantially versus time at 70 wt% bead loading. In contrast, at 50 wt% loading, >45% of the cells entered apoptosis or necrosis at 30 min post-mixing. For the immediate addition group, % apoptosis (or necrosis) decreased slightly at 3 h, while for the delayed addition group % apoptosis (or necrosis) continued to increase. As shown in the contour plots (Fig. 6C–D), the percentage of cells entering apoptosis or necrosis increased with increasing reaction time and decreasing permeability. As anticipated, permeability exhibited only a modest effect on % apoptosis (or necrosis) at 10 min post-mixing, since the scaffold had not yet formed. However, at 3 h % apoptosis increased with permeability, approaching 50% at the lowest permeability. These observations point to both chemical reaction products and scaffold permeability as key factors limiting cell survivability.

3.5. Long-term culture of encapsulated cells in vitro

The ability of BMSCs to attach to the scaffold *in vitro* was investigated for both Alg and o-Alg beads for the conditions at which cell survivability was highest: 70% loading and 3 min delayed addition. The beads exhibited a folded surface morphology (Fig. S4A) and nanoscale mesh size (19 ± 3 nm for Alg and 65 ± 3 nm for o-Alg beads [42,43]) consistent with findings from previous studies [44]. After encapsulation, cells exhibited a rounded morphology (Fig. S4B), since there are no adhesive ligands to facilitate attachment to the Alg. After 7 days in culture, cells (stained green with a cytoplasmic dye) remained clustered within the Alg beads, with few cells appearing adjacent or adherent to the PUR scaffold (stained blue, Fig. 7A), which suggests that cells could not escape the slow-degrading, nanostructured mesh. In contrast, PUR scaffolds embedded with o-Alg beads showed evidence of cell release from the beads and increasing numbers of cells lining the PUR surface with time. Similarly, SEM analysis showed that cells were attached to the surface of PUR scaffolds embedded with o-Alg beads (Fig. 7B). Thus, loading the scaffold with 70% o-Alg beads not only increased permeability and pore interconnectivity (Fig. 6B–C), but also supported release of cells from the beads and consequent attachment to the scaffold. These observations are consistent with the notion that o-Alg is a temporary protective shield that degrades within 1–2 days (Fig. S5), releasing the cells so they can attach to the PUR scaffold. To determine whether MSCs retained their pluripotency after the reaction, scaffolds with o-Alg beads were cultured in growth, adipogenic, or osteogenic medium for 21 days. Compared to cells cultured in growth medium, cells cultured in adipogenic medium showed higher Oil Red O absorbance, while cells cultured in osteogenic medium showed higher alizarin red dye absorbance (Fig. 7C). Thus, after exposure to the chemical reaction, BMSCs retained their potential to differentiate to adipocytes or osteoblasts.

3.6. In vivo delivery of BMSCs encapsulated in injectable PUR scaffolds

To investigate the ability of the cells to survive the injection and generate new extracellular matrix *in vivo*, a proof-of-concept experiment was performed in full-thickness excisional skin wounds in Sprague–Dawley (SD) rats [16]. BMSCs from male SD rats were delivered to wounds in female rats, and SRY (sex determining region Y, Sox9) immunohistochemical staining was

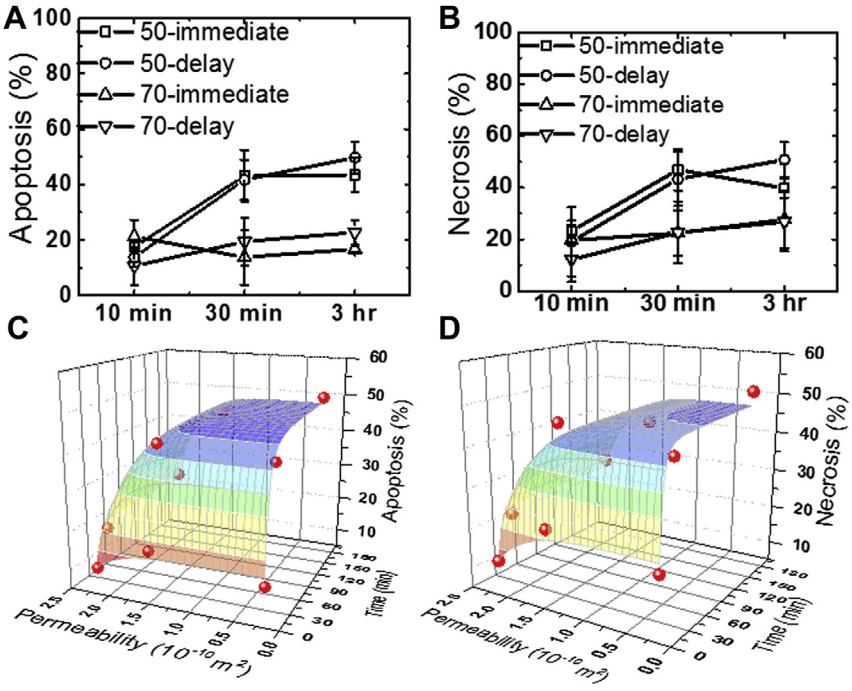

Fig. 6. Effects of bead loading and timing of bead addition on cell viability at late time points. The percentage of cells undergoing apoptosis (A) or necrosis (B) was measured at 10 min, 30 min, and 3 h as a function of bead loading (50 or 70 wt% Alg beads) and timing of addition (immediate or delayed for 3 min). (C–D) Contour plots showing the percentage of cells undergoing apoptosis (C) or necrosis (D) as a function of reaction time (10 min, 30 min, or 3 h) and scaffold permeability. Cell survivability decreases with increasing reaction time and decreasing permeability.

performed to track transplanted cells. PUR scaffolds embedded with Alg beads with or without cells were extruded from the wounds after 7 days (data not shown) due to persistence of Alg and consequent low porosity. In contrast, transplanted BMSCs (10^5 cells/ml equivalent to 2×10^4 cells/scaffold) encapsulated in o-Alg and embedded in injectable (Inj + BMSC) or implantable (Impl + BMSC) PUR scaffolds survived for at least 7 days (Fig. 8A, B). High-magnification (20X, Fig. 9A, B) images from trichrome staining revealed degradation of o-Alg to form new pores throughout the scaffold (PUR, light gray), while some fragments of o-Alg (A, green acellular material) remained. New extracellular matrix (green tint, M) was deposited as early as day 4. The Inj + BMSC group showed significantly more deposition of new extracellular matrix at both time points compared to the Inj (injectable with no cells) or the Impl + BMSC (implanted scaffold seeded with cells) groups (Fig. 9C). To investigate the mechanism by which transplanted BMSCs enhanced deposition of new matrix, we measured the prevalence of $Ki67^+$ proliferating cells and deposition of collagen IV (a marker of angiogenesis) in Inj and Inj + BMSC scaffolds by immunohistochemical staining. Inj + BMSC scaffolds showed significantly more $Ki67^+$ proliferating cells (Fig. 9D) and increased collagen IV accumulation (Fig. 9E) compared to Inj scaffolds. Taken together, these observations indicate that transplanted BMSCs not only survived the chemical reaction, but also stimulated cell proliferation and angiogenesis after transplantation *in vivo*.

4. Discussion

In this study, we designed injectable PUR scaffolds for local transplantation of viable cells for tissue repair and restoration by encapsulating cells in degradable o-Alg beads prior to embedding in the reactive polymer. In contrast to hydrogels that utilize water-soluble initiators [17,18] and macromers [19–21] to facilitate cell encapsulation from aqueous suspensions, direct encapsulation of cells in reactive hydrophobic polymers is confounded by their low (<5%) swelling in water and generation of chemical by-products and heat [7]. Two factors limited cell survivability *in vitro*: (1) generation of CO_2 and heat by the chemical reaction prior to gelation, and (2) permeability of the scaffolds after gelation. Delayed (3 min) addition of the o-Alg beads at a loading of 70% balanced the requirements for minimal exposure of cells to reaction products, high permeability for transport of nutrients and wastes, and mechanical integrity of the scaffolds. Under these conditions, PUR scaffolds injected with encapsulated BMSCs promoted increased extracellular matrix deposition *in vivo* compared to both injected acellular scaffolds and implanted scaffolds seeded with BMSCs, and they did so without biofunctionalization of the scaffold with expensive peptides, growth factors, or other biologics.

Encapsulation of cells in Alg beads of sufficient size provided a barrier to diffusion of CO_2 and heat prior to gelation (10 min). This observation is consistent with a previous study reporting that acellular PUR scaffolds reach the reaction exotherm at 3 min post-mixing [15]. While Alg protected the cells from the chemical reaction prior to gelation, the persistence of Alg after gelation hindered attachment of cells to the scaffolds *in vitro* (Fig. 7A–B) and tissue ingrowth *in vivo*. These observations are in agreement with a previous study reporting that cells encapsulated in Alg beads and embedded in a CPC failed to release from beads after 14 days in culture [34]. Thus, slow dissolution of Alg beads precludes the formation of interconnected macropores (>10 μm) [36,45]. Partial oxidation to o-Alg renders it susceptible to hydrolysis [28,46], which has prompted the use of o-Alg as a degradable carrier for MSCs. Delivery of human adipose stem cells from o-Alg hydrogels with a degradation time of ~40 days promoted generation of new adipose tissue in mice [47]. In another study, MSCs encapsulated in o-Alg beads and mixed with a calcium phosphate cement (CPC) provided mechanical protection during mixing [48,49]. However, the utility of o-Alg as a temporary barrier to diffusion of harmful

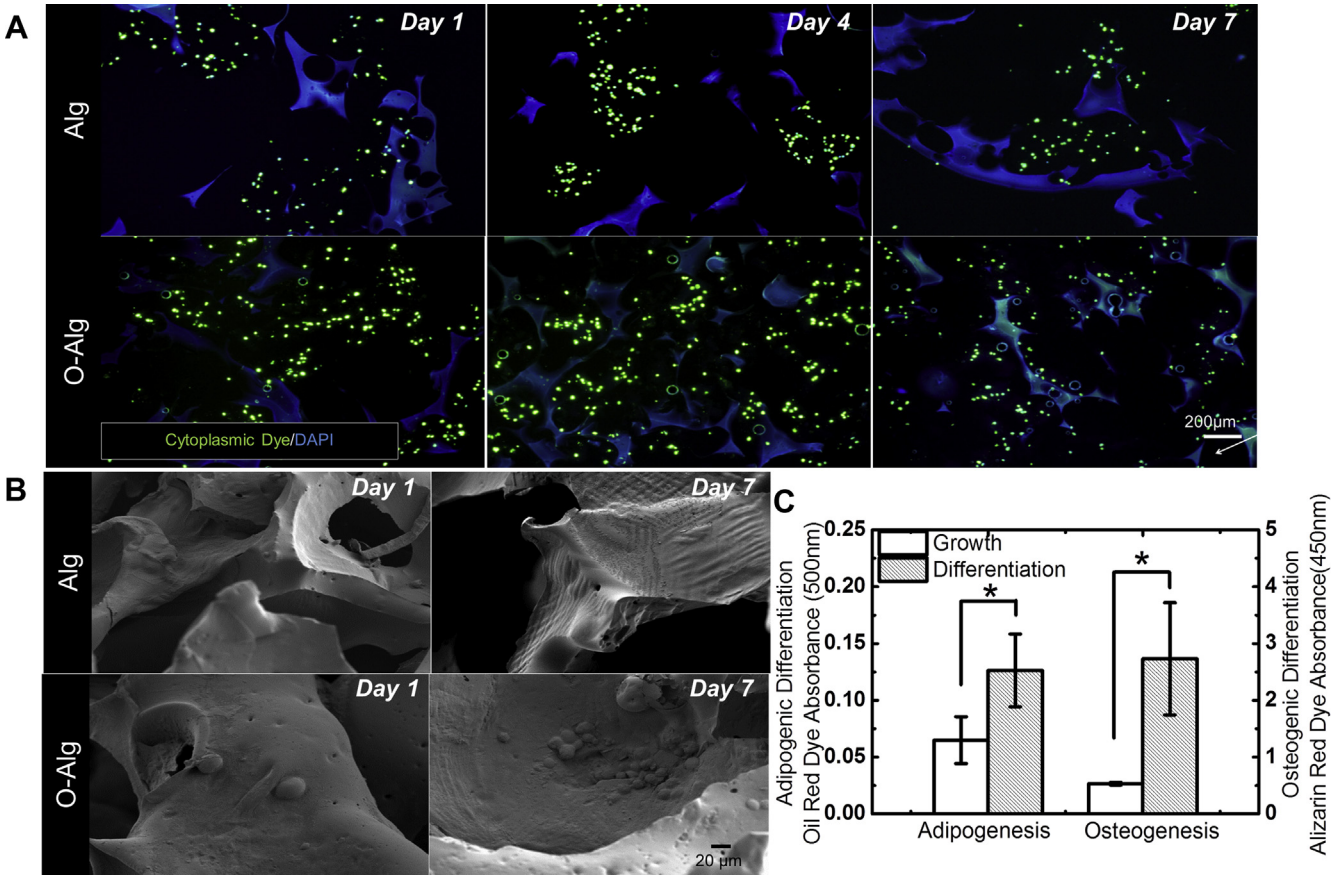

Fig. 7. *In vitro* culture of BMSCs on injectable PUR scaffolds *in vitro*. (A) Representative histological sections stained with the cytoplasmic dye carboxyfluorescein diacetate (CFDA, green) and DAPI (blue) of PUR scaffolds loaded with 70 wt% 500 μm Alg or o-Alg beads show viable rat BMSCs at days 1, 4, and 7. Cells are stained green and the scaffold is stained blue. (B) Representative SEM images of PUR scaffolds loaded with 70 wt% 500 μm o-Alg beads showed cells attached to the scaffold after 7 days, while few attached cells were observed for scaffolds loaded with Alg beads. (C) Osteogenic (measured by Alizarin red absorption) and adipogenic (measured by Oil Red O absorption) differentiation of BMSCs encapsulated in polyurethane foams. (For interpretation of the references to color in this figure legend, the reader is referred to the web version of this article.)

chemical reaction products, which was the subject of the present study, has not been systematically investigated.

Considering the optimal pore size of 90–360 μm reported for cellular infiltration and new tissue ingrowth [50], the diameter of the o-Alg beads was initially targeted at ~350 μm. However, when 500 μm beads were immediately mixed with the reactive polymer, only 30% of the cells survived at 10 min (Fig. 3B–C). As shown in Fig. 4C, generation of both CO_2 and heat outside the region bounded by $Q_{10} > 0.4$ J cm^{-2} and $n_{CO2,10} > 0.08$ mmol cm^{-2} (calculated at 10 min from the chemical kinetics) resulted in excessive cell death. Delayed addition of o-Alg beads reduced CO_2 generation below 0.08 mmol cm^{-2}, thereby increasing acute survivability of cells encapsulated in 500 μm beads to levels exceeding 80% (Fig. 4C). These observations are consistent with a previous study reporting that the viability of cells encapsulated in fibrin-alginate beads embedded in an injectable CPC decreased as the concentration of $NaHCO_3$ (reacting with citric acid to produce CO_2) increased from 15 to 30% [49]. Considering that the bicarbonate-citric acid reaction is endothermic, cell death in this previous study was likely caused by CO_2.

An important unanswered question is whether the cells die in response to a cumulative increase in temperature (or CO_2 concentration) or the rate at which these parameters are changing. Quantifying the relative contributions of CO_2 and heat generation to cell death both prior to and after gelation requires solution of the unsteady state heat conduction and CO_2 diffusion equations for both Alg (A) and polymer (PUR) phases [51]:

$$\begin{aligned}
\frac{\partial T_A}{\partial t} &= \alpha_A \nabla^2 T_A \\
\frac{\partial T_{PUR}}{\partial t} &= \alpha_{PUR} \nabla^2 T_{PUR} + \frac{Q(t)}{\rho_{PUR} C_{P,PUR}} \\
\frac{\partial c_{CO_2,A}}{\partial t} &= D_{CO_2,A} \nabla^2 c_{CO_2,A} \\
\frac{\partial c_{CO_2,PUR}}{\partial t} &= D_{CO_2,PUR} \nabla^2 c_{CO_2,PUR} + r_{CO_2,PUR}
\end{aligned} \tag{9}$$

where $\alpha = \kappa/\rho C_p$ is the thermal diffusivity, κ is the thermal conductivity, C_p is the heat capacity, $Q(t)$ is the heat generated by the chemical reaction (Eq. (6)), c_{CO2} is the concentration of carbon dioxide, and D_{CO2} is the diffusivity of CO_2. Both $D_{CO2,A}$ and α_A are anticipated to increase with increasing mesh size, resulting in steeper temperature and CO_2 gradients in the beads. The exact solution of the unsteady state heat conduction and CO_2 diffusion equations is outside the scope of this study, but several observations can be made from the apoptosis/necrosis kinetic data (Fig. 6C–D). The percentage of cells entering apoptosis or necrosis increased from 10 min to 3 h for all scaffolds, including highly permeable ($>2 \times 10^{-10}$ m^2) PUR scaffolds with minimal transport limitations, suggesting that the cells did not recover from the initial exposure to heat and CO_2. Furthermore, the percentages of apoptotic and necrotic cells were comparable at all time points and permeabilities. The majority of damaged cells stained positive for both apoptotic and necrotic markers, which further confirms that

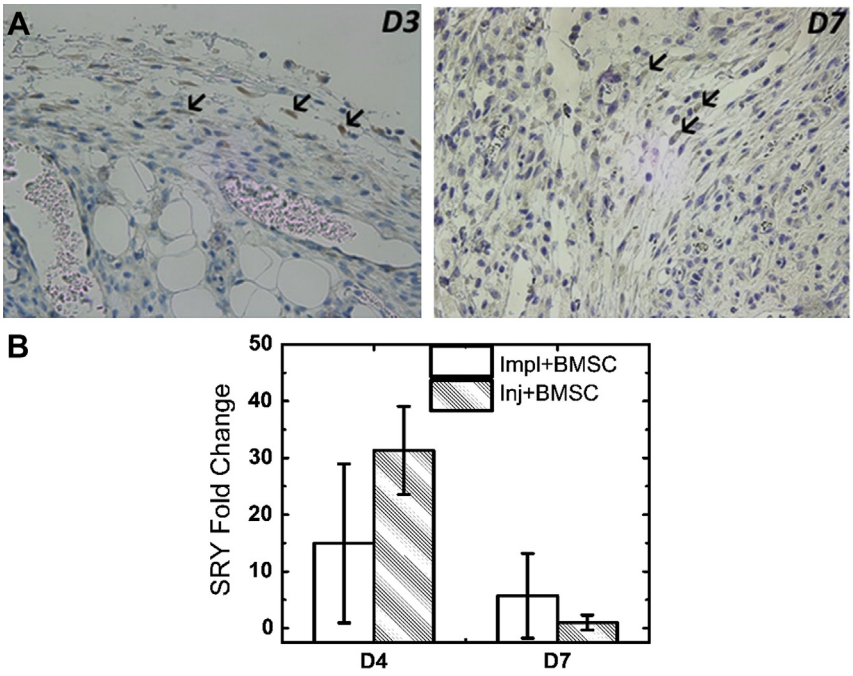

Fig. 8. Rat BMSCs encapsulated in 500 μm o-Alg beads embedded in PUR scaffolds survive transplantation for up to 7 days in a rat excisional wound model. (A) SRY (sex determining region Y, Sox9) immunohistochemical staining revealed the presence of male donor rat BMSCs in wounds on female rats (black arrows) at day 7 (40× magnification). (B) qRT-PCR measurements of *SRY* expression show that cells survived for up to 7 days in implanted (Impl + BMSC) and injected (Inj + BMSC) scaffolds.

cells did not recover from the initial exposure to reaction products. Finally, cell survival after gelation (30 min–3 h) improved dramatically in highly permeable ($>2 \times 10^{-10}$ m^2) scaffolds. These observations suggest that exposure to heat and CO_2 regulates cell survival prior to gelation, while scaffold permeability controls cell survival after gelation.

Potential hurdles to clinical translation of the injectable hydrophobic scaffold approach include the requirements of specialized encapsulation equipment and delayed addition of the o-Alg beads, which increases the duration of the surgical procedure. In this study, the maximum delay for bead addition was 6 min, beyond which time the beads could not be uniformly mixed with the reactive PUR. The maximum delay is determined by the working time, which was targeted at 20 min to be consistent with the handling properties reported for calcium phosphate cements [37], a clinically relevant class of injectable and settable biomaterials. As an alternative to delayed addition, the rate of CO_2 generation can be controlled by tuning the gel:blow (k_G/k_B) ratio. For the LTI-PEG prepolymer and FeAA catalyst used in this study, the gel:blow ratio was 6.4 (Table 1), which is substantially greater than the value of ~0.05 reported for a triethylene diamine catalyst [7] but not large enough to obviate the need for delayed addition of the beads. In contrast, HDIt exhibited a gel:blow ratio of 13.4 at the lowest catalyst level (Table 1), which was sufficiently high that delayed addition of the beads was not required to achieve high viability. These observations point to the gel:blow ratio as a key parameter for maintaining high cell survivability without delayed addition of the beads. The adverse effects of the polymerization on cell survivability could be further reduced by slowing the gelling reaction, which would decrease the rate of heat generation. However, the advantageous effects of slowing the gelling reaction on cell survival at early time points must be balanced against the potentially adverse effects of longer *in situ* setting times on both the handling properties as well as the mechanical stability of the PUR scaffold after injection.

In a proof-of-concept *in vivo* experiment, injected scaffolds showed comparable cell survival to implanted scaffolds (Fig. 8B). However, the Inj + BMSC group showed significantly more new granulation tissue compared to both the Impl + BMSC and Inj (no cells) groups (Fig. 9C). To investigate the mechanism by which transplanted BMSCs enhanced healing, we measured the number of Ki67$^+$ proliferating cells and deposition of collagen IV, a basement membrane protein that marks capillary endothelium in granulation tissue that forms within embedded scaffolds. The area % of Ki67$^+$ cells was significantly higher in the Inj + BMSC group compared to the Inj group on days 4 and 7 (Fig. 9D). Furthermore, the area% collagen IV was significantly higher in the Inj + BMSC group on days 7 and 14, despite the fact that the transplanted cells survived for only 7 days. These observations are consistent with the notion of trophic activity, by which MSCs influence healing by the secretion of growth factors and cytokines that stimulate proliferation of tissue-intrinsic progenitor cells as well as angiogenesis [52,53]. Using this adaptable and versatile PUR carrier, BMSCs can be encapsulated in o-Alg beads directly after harvesting, mixed with the reactive polymer, and injected into defects of varying sizes and complex shapes as a site-directed therapeutic [54].

5. Conclusion

Injectable PUR scaffolds embedded with bone marrow-derived MSCs encapsulated in o-Alg were designed to promote peripheral tissue infiltration in rat subcutaneous wound model. MSCs were encapsulated in o-Alg before the PUR reaction to enhance cell survivability. After incorporation, o-Alg beads subsequently degraded to form interconnected macropores that supported cellular migration, proliferation, and deposition of new extracellular matrix *in vitro* and *in vivo*. These properties underscore the potential utility of PUR scaffolds as a versatile, clinically relevant, and functionally-significant injectable cell delivery system for regenerative medicine applications.

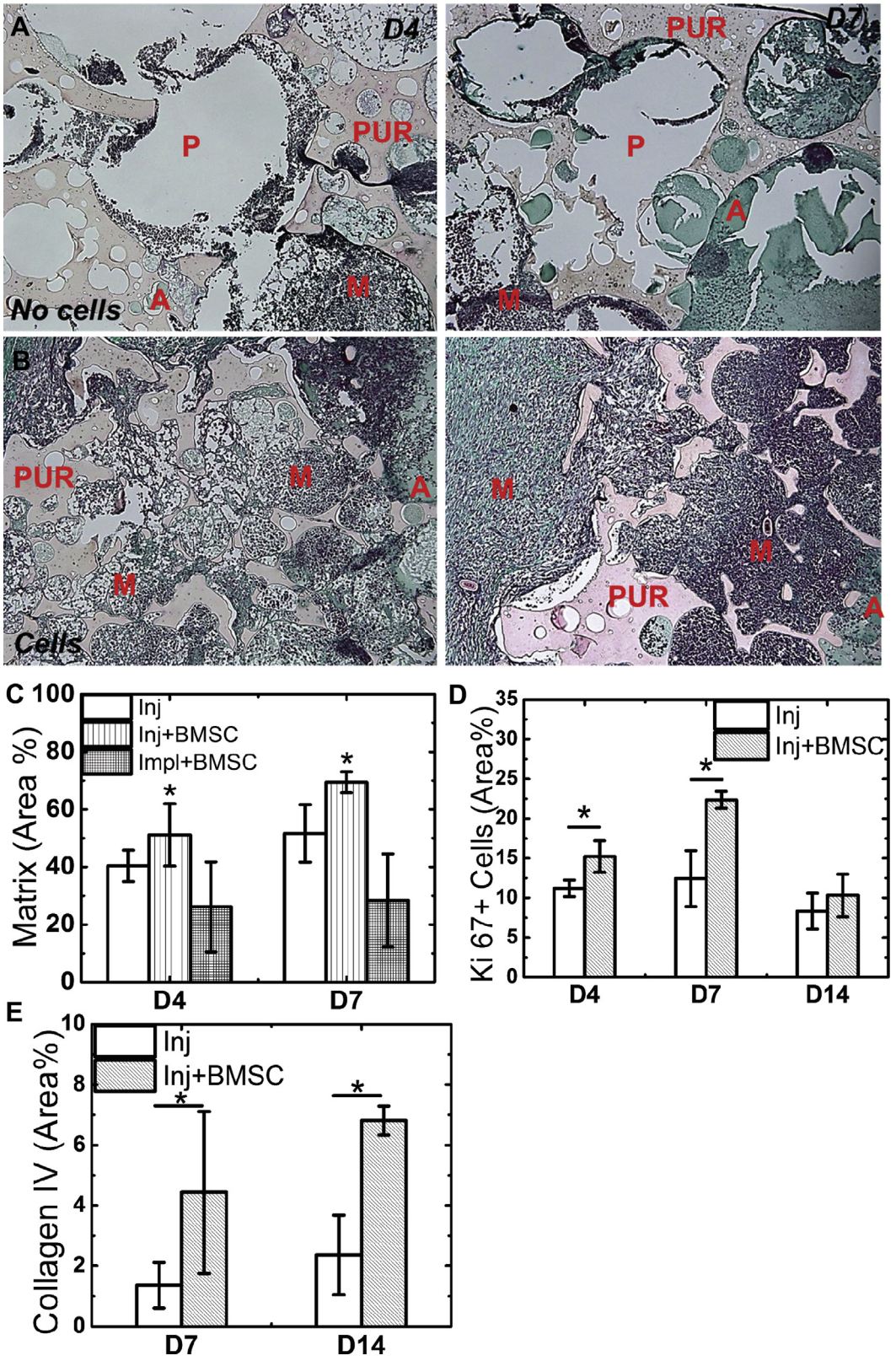

Fig. 9. Rat BMSCs encapsulated in 500 μm o-Alg beads embedded in PUR scaffolds enhance deposition of new extracellular matrix in a rat excisional wound model. (A–B) High-magnification (20×) images of histological sections 7 days after injection of PUR scaffolds without (A) or with (B) 10^5 rat BMSCs/ml encapsulated in o-Alg beads into 10-mm excisional wounds in rats. Local cell delivery increased deposition of new extracellular matrix (**M**). O-Alg beads (**A**) degraded to form macropores (**P**), resulting in infiltration of cells and ingrowth of granulation tissue along the surface of the residual polyurethane (**PUR**) scaffold. (C) Histomorphometric analysis showed that Inj + BMSC scaffolds supported significantly greater ingrowth of extracellular matrix at days 4 and 7 compared to the injected acellular (Inj) and cellular implant (Impl + BMSC) controls. (D–E) $Ki67^+$ proliferating cells (D) and collagen IV (E) are higher in Inj + BMSC scaffolds at days 4 and 7 compared to the acellular Inj control. * denotes significant differences between the blank and BMSC groups, $p < 0.05$.

Acknowledgments

The authors acknowledge Frank Rauh at FMC Novamatrix for helpful discussions on preparation of partially oxidized alginate. Financial support was provided by the Orthopaedic Extremity Trauma Research Program (DOD W81XWH-07-1-0211), the National Institute of Arthritis and Musculoskeletal and Skin Diseases (AR056138), and the Department of Veterans Affairs. The content is solely the responsibility of the authors and does not necessarily represent the official views of the National Institutes of Health or the Department of Veterans Affairs.

Appendix A. Supplementary data

Supplementary data related to this article can be found at http://dx.doi.org/10.1016/j.biomaterials.2015.03.010.

References

[1] Burdick JA, Anseth KS. Photoencapsulation of osteoblasts in injectable RGD-modified PEG hydrogels for bone tissue engineering. Biomaterials 2002;23:4315–23.
[2] Cleland JG, Coletta AP, Abdellah AT, Cullington D, Clark AL, Rigby AS. Clinical trials update from the American Heart Association 2007: CORONA, RethinQ, MASCOT, AF-CHF, HART, MASTER, POISE and stem cell therapy. Eur J Heart Fail 2008;10:102–8.
[3] Horwitz EM, Prockop DJ, Fitzpatrick LA, Koo WW, Gordon PL, Neel M, et al. Transplantability and therapeutic effects of bone marrow-derived mesenchymal cells in children with osteogenesis imperfecta. Nat Med 1999;5:309–13.
[4] Orlic D, Kajstura J, Chimenti S, Jakoniuk I, Anderson SM, Li B, et al. Bone marrow cells regenerate infarcted myocardium. Nature 2001;410:701–5.
[5] Salinas CN, Anseth KS. Mesenchymal stem cells for craniofacial tissue regeneration: designing hydrogel delivery vehicles. J Dent Res 2009;88:681–92.
[6] Kretlow JD, Klouda L, Mikos AG. Injectable matrices and scaffolds for drug delivery in tissue engineering. Adv Drug Deliv Rev 2007;59:263–73.
[7] Page JM, Prieto EM, Dumas JE, Zienkiewicz KJ, Wenke JC, Brown-Baer P, et al. Biocompatibility and chemical reaction kinetics of injectable, settable polyurethane/allograft bone biocomposites. Acta Biomater 2012;8:4405–16.
[8] Nguyen KT, West JL. Photopolymerizable hydrogels for tissue engineering applications. Biomaterials 2002;23:4307–14.
[9] Guelcher SA, Srinivasan A, Dumas JE, Didier JE, McBride S, Hollinger JO. Synthesis, mechanical properties, biocompatibility, and biodegradation of polyurethane networks from lysine polyisocyanates. Biomaterials 2008;29:1762–75.
[10] Zhang J-Y, Beckman EJ, Piesco NJ, Agarwal S. A new peptide-based urethane polymer: synthesis, biodegradation, and potential to support cell growth in vitro. Biomaterials 2000;21:1247–58.
[11] Hafeman AE, Zienkiewicz KJ, Zachman AL, Sung HJ, Nanney LB, Davidson JM, et al. Characterization of the degradation mechanisms of lysine-derived aliphatic poly(ester urethane) scaffolds. Biomaterials 2011;32:419–29.
[12] Martin JR, Gupta MK, Page JM, Yu F, Davidson JM, Guelcher SA, et al. A porous tissue engineering scaffold selectively degraded by cell-generated reactive oxygen species. Biomaterials 2014;35:3766–76.
[13] Hafeman A, Li B, Yoshii T, Zienkiewicz K, Davidson J, Guelcher S. Injectable biodegradable polyurethane scaffolds with release of platelet-derived growth factor for tissue repair and regeneration. Pharm Res 2008;25:2387–99.
[14] Guelcher SA. Biodegradable polyurethanes: synthesis and applications in regenerative medicine. Tissue Eng B Rev 2008;14:3–17.
[15] Guelcher S, Srinivasan A, Hafeman A, Gallagher K, Doctor J, Khetan S, et al. Synthesis, in vitro degradation, and mechanical properties of two-component poly(ester urethane)urea scaffolds: effects of water and polyol composition. Tissue Eng 2007;13:2321–33.
[16] Adolph EJ, Hafeman AE, Davidson JM, Nanney LB, Guelcher SA. Injectable polyurethane composite scaffolds delay wound contraction and support cellular infiltration and remodeling in rat excisional wounds. J Biomed Mater Res A 2012;100A:450–61.
[17] Mann BK, Gobin AS, Tsai AT, Schmedlen RH, West JL. Smooth muscle cell growth in photopolymerized hydrogels with cell adhesive and proteolytically degradable domains: synthetic ECM analogs for tissue engineering. Biomaterials 2001;22:3045–51.
[18] Bryant SJ, Nuttelman CR, Anseth KS. Cytocompatibility of UV and visible light photoinitiating systems on cultured NIH/3T3 fibroblasts in vitro. J Biomater Sci Polym Ed 2000;11:439–57.
[19] Kim IS, Jeong YI, Kim SH. Self-assembled hydrogel nanoparticles composed of dextran and poly(ethylene glycol) macromer. Int J Pharm 2000;205:109–16.
[20] Martens P, Anseth KS. Characterization of hydrogels formed from acrylate modified poly(vinyl alcohol) macromers. Polymer 2000;41:7715–22.
[21] Bulpitt P, Aeschlimann D. New strategy for chemical modification of hyaluronic acid: preparation of functionalized derivatives and their use in the formation of novel biocompatible hydrogels. J Biomed Mater Res 1999;47:152–69.
[22] Kloxin AM, Kloxin CJ, Bowman CN, Anseth KS. Mechanical properties of cellularly responsive hydrogels and their experimental determination. Adv Mater 2010;22:3484–94.
[23] Boerckel JD, Kolambkar YM, Dupont KM, Uhrig BA, Phelps EA, Stevens HY, et al. Effects of protein dose and delivery system on BMP-mediated bone regeneration. Biomaterials 2011;32:5241–51.
[24] Phelps EA, Enemchukwu NO, Fiore VF, Sy JC, Murthy N, Sulchek TA, et al. Maleimide cross-linked bioactive PEG hydrogel exhibits improved reaction kinetics and cross-linking for cell encapsulation and in situ delivery. Adv Mater 2012;24:64–70. 2.
[25] Lutolf MP, Lauer-Fields JL, Schmoekel HG, Metters AT, Weber FE, Fields GB, et al. Synthetic matrix metalloproteinase-sensitive hydrogels for the conduction of tissue regeneration: engineering cell-invasion characteristics. Proc Natl Acad Sci U. S. A 2003;100:5413–8.
[26] Hwang CM, Sant S, Masaeli M, Kachouie NN, Zamanian B, Lee SH, et al. Fabrication of three-dimensional porous cell-laden hydrogel for tissue engineering. Biofabrication 2010;2:035003.
[27] Scott EA, Nichols MD, Kuntz-Willits R, Elbert DL. Modular scaffolds assembled around living cells using poly(ethylene glycol) microspheres with macroporation via a non-cytotoxic porogen. Acta Biomater 2010;6:29–38.
[28] Bouhadir KH, Lee KY, Alsberg E, Damm KL, Anderson KW, Mooney DJ. Degradation of partially oxidized alginate and its potential application for tissue engineering. Biotechnol Prog 2001;17:945–50.
[29] Balakrishnan B, Joshi N, Jayakrishnan A, Banerjee R. Self-crosslinked oxidized alginate/gelatin hydrogel as injectable, adhesive biomimetic scaffolds for cartilage regeneration. Acta Biomater 2014;10:3650–63.
[30] Moghadam H, Samimi M, Samimi A, Khorram M. Electro-spray of high viscous liquids for producing mono-sized spherical alginate beads. Particuology 2008;6:271–5.
[31] Guelcher SA, Patel V, Gallagher KM, Connolly S, Didier JE, Doctor JS, et al. Synthesis and in vitro biocompatibility of injectable polyurethane foam scaffolds. Tissue Eng 2006;12:1247–59.
[32] Dumas JE, Zienkiewicz K, Tanner SA, Prieto EM, Bhattacharyya S, Guelcher S. Synthesis and characterization of an injectable allograft Bone/polymer composite bone void filler with tunable mechanical properties. Tissue Eng Part A 2010;16:2505–18.
[33] Zhao W, Fierro V, Pizzi A, Du G, Celzard A. Effect of composition and processing parameters on the characteristics of tannin-based rigid foams. Part II: physical properties. Mater Chem Phys 2010;123:210–7.
[34] Zhao L, Weir MD, Xu HH. An injectable calcium phosphate-alginate hydrogel-umbilical cord mesenchymal stem cell paste for bone tissue engineering. Biomaterials 2010;31:6502–10.
[35] Guvendiren M, Lu HD, Burdick JA. Shear-thinning hydrogels for biomedical applications. Soft Matter 2012;8:260–72.
[36] Bencherif SA, Sands RW, Bhatta D, Arany P, Verbeke CS, Edwards DA, et al. Injectable preformed scaffolds with shape-memory properties. Proc Natl Acad Sci U. S. A 2012;109:19590–5.
[37] Bohner M. Design of ceramic-based cements and putties for bone graft substitution. Eur Cell Mater 2010;20:1–12.
[38] Sperling LH. Introduction to physical polymer science. 3rd ed. New York: Wiley-Interscience; 2001.
[39] Parnell S, Min K, Cakmak M. Kinetic studies of polyurethane polymerization with Raman spectroscopy. Polymer 2003;44:5137–44.
[40] Lovering EG, Laidler KJ. Thermochemical studies of some alcohol-isocyanate reactions. Can J Chem 1962;40:26–30.
[41] Gibson LJ, Ashby MF. Cellular solids: structure and properties. Cambridge University Press; 1997.
[42] Lee BH, Li B, Guelcher SA. Gel microstructure regulates proliferation and differentiation of MC3T3-E1 cells encapsulated in alginate beads. Acta Biomater 2012;8:1693–702.
[43] Kong HJ, Kaigler D, Kim K, Mooney DJ. Controlling rigidity and degradation of alginate hydrogels via molecular weight distribution. Biomacromolecules 2004;5:1720–7.
[44] Sarker B, Papageorgiou DG, Silva R, Zehnder T, Gul-E-Noor F, Bertmer M, et al. Fabrication of alginate–gelatin crosslinked hydrogel microcapsules and evaluation of the microstructure and physico-chemical properties. J Mater Chem B 2014;2:1470–82.
[45] Han LH, Lai JH, Yu S, Yang F. Dynamic tissue engineering scaffolds with stimuli-responsive macroporosity formation. Biomaterials 2013;34:4251–8.
[46] Boontheekul T, Kong HJ, Mooney DJ. Controlling alginate gel degradation utilizing partial oxidation and bimodal molecular weight distribution. Biomaterials 2005;26:2455–65.
[47] Kim WS, Mooney DJ, Arany PR, Lee K, Huebsch N, Kim J. Adipose tissue engineering using injectable, oxidized alginate hydrogels. Tissue Eng Part A 2012;18:737–43.
[48] Tang M, Chen W, Weir MD, Thein-Han W, Xu HH. Human embryonic stem cell encapsulation in alginate microbeads in macroporous calcium

phosphate cement for bone tissue engineering. Acta Biomater 2012;8:3436–45.
[49] Chen W, Zhou H, Tang M, Weir MD, Bao C, Xu HH. Gas-foaming calcium phosphate cement scaffold encapsulating human umbilical cord stem cells. Tissue Eng Part A 2012;18:816–27.
[50] Wang H, Pieper J, Peters F, van Blitterswijk CA, Lamme EN. Synthetic scaffold morphology controls human dermal connective tissue formation. J Biomed Mater Res A 2005;74:523–32.
[51] Bird R, Stewart W, Lightfoot E. Transport phenomena. New York: Wiley; 1960.
[52] Caplan AI, Dennis JE. Mesenchymal stem cells as trophic mediators. J Cell Biochem 2006;98:1076–84.
[53] Caplan AI. Why are MSCs therapeutic? New data: new insight. J Pathol 2009;217:318–24.
[54] Dennis JE, Cohen N, Goldberg VM, Caplan AI. Targeted delivery of progenitor cells for cartilage repair. J Orthop Res 2004;22:735–41.